ELSEVIER

Surface Science 429 (1999) 133–142

surface science

www.elsevier.nl/locate/susc

Theoretical study of the decomposition of HCOOH on an MgO(100) surface

Masami Lintuluoto [a], Hiroshi Nakatsuji [b, c,*], Masahiko Hada [b], Hiroyoshi Kanai [a]

[a] *Department of Environmental Information, Faculty of Human Environment, Kyoto Prefectural University, Shimogamo hanki-cho, Sakyo-ku, Kyoto 606, Japan*

[b] *Department of Synthetic Chemistry and Biological Chemistry, Faculty of Engineering, Kyoto University, Sakyo-ku, 606-01 Kyoto, Japan*

[c] *Institute of Fundamental Chemistry, Nishihiraki-cho, Sakyo-ku, Kyoto 606, Japan*

Received 7 July 1997; accepted for publication 19 January 1999

Abstract

We present here a theoretical investigation of the mechanism of the decomposition of formic acid on perfect and defective MgO(100) surfaces using the ab initio molecular orbital method. The decomposition reaction does not occur on a perfect surface, but is feasible on defect surfaces: the surface with an O^{2-} vacancy is more favorable than the surface with an O vacancy. Although the mechanism is different from that in the gas phase, C–H and C–O bond cleavages occur at the same time in the transition state, as in the gas phase. The carbonyl O atom moves into the vacancy to form an intermediate structure. The intermediate is more stable by 41.7 kcal mol^{-1} at the UMP2 level than the bridging structure. The C–H interacts with the lattice O atom to form a surface OH species. The interaction between the C–H and lattice Mg atoms is repulsive. The energy barrier is 28.3 kcal mol^{-1} and the overall reaction is endothermic by 48.9 kcal mol^{-1} at the UMP2 level.

Keywords: Ab initio molecular method; Formic acid; MgO(100) surface

1. Introduction

It is well known that metal oxides are good catalysts for a variety of chemical processes [1–26]. For example, methanol, formaldehyde and formic acid readily decompose on MgO catalysts [7,8,10–12]. Formate anion has been suggested to be a surface intermediate in various water gas shift reactions on metal oxide surfaces [13–16]. Formic acid is adsorbed dissociatively on metal and metal oxide surfaces at room temperature and gives formate anion and surface hydroxyl species [4–6,11,18–24]. Three structures have been suggested for the formate anion adsorbed on metal oxide surfaces [4–6,11,18–24]; bridging, bidentate, and unidentate structures (Fig. 1). The formic acid adsorbed on metal and metal oxide surfaces decomposes to produce H_2O+CO or H_2+CO_2 [1–6,12–24]. Many attempts have been made to clarify the active species, the reactivities and the selectivities of catalysts in the decomposition of formic acid. The hydrogenation is favored on MgO powder in the reaction under continuous flow of reactant [25], while the reaction under ultrahigh

* Corresponding author. Fax: +81 75 753 5910.
E-mail address: hiroshi@sbchem.kyoto-u.ac.jp (H. Nakatsuji)

0039-6028/99/$ – see front matter
PII: S0039-6028(99)00357-X

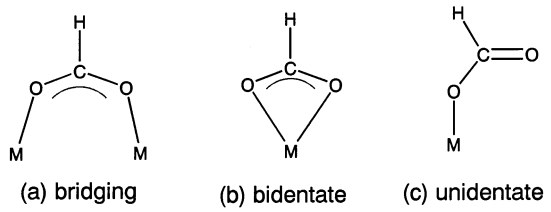

Fig. 1. Three possible geometries of a formate anion on a surface.

vacuum (UHV) conditions over the surface of an MgO single crystal was found to favor dehydration [26].

The decomposition reaction of formic acid in the gas phase has been reported previously using theoretical methods [27,28]. The structures in the transition state and the activation energies for hydrogenation and hydration reactions have been reported as shown in Fig. 2.

However, many questions remain unanswered, such as the active site, the structure of the adsorbed species, and the mechanism of the surface reaction. Theoretical studies have been reported for hydrogen chemisorption on a MgO surface [28–32] and other metal oxide surfaces [33–40] and for the adsorption of formic acid on metal [17] and bimetal [41] surfaces. Previously, we theoretically studied the adsorption of formic acid and its surface reactions on MgO(001) [42] and ZnO($10\bar{1}0$) [43,44] surfaces. We used an Mg_8O_8 cluster embedded in a Madelung potential to simulate MgO(100) and found that formic acid is dissociatively adsorbed to form the formate anion and a surface OH species with a low energy barrier on a MgO(100) surface. The favorable structure for the formate anion on a MgO(100) surface was the bridging structure [42]. Within the temperature range of the decomposition reaction, formic acid is dissociatively adsorbed into the formate anion and a surface OH species on MgO surfaces [11,12]. Therefore, we adopted adsorbed bridging formate anion and surface OH species for the initial geometry, as shown in Fig. 3.

Some investigations of the reactive behavior of the well-defined MgO(100) surfaces indicated a close association of catalytic activity and the presence of coordinatively unsaturated adsorption sites rather than the saturated five-fold coordination sites of the ideal MgO(100) surface [45–47]. Peng and Barteau have reported that formaic acid and acetic acids adsorb on the five-fold coordinated Mg–O site pairs of the MgO(100) surface in the form of carboxylates and the thermal decomposition under UHV conditions proceeds via dehydration alone [26]. They reported the dissociative adsorption of the weaker Brønsted acid such as CH_3OH in the subsequent paper [48], and suggested that the ideal five-fold sites of MgO(100) may become populated with the adsorbed species via a mechanism akin to spillover, involving an initial activation of the corresponding acid at a defect site followed by later migration of the

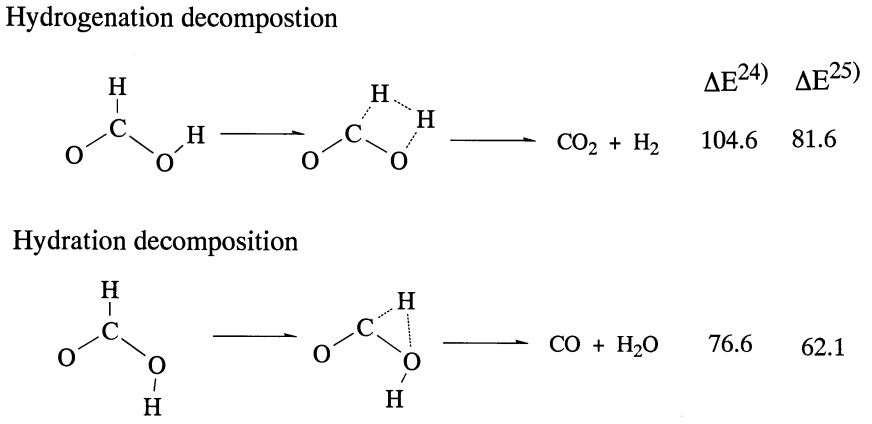

Fig. 2. The mechanisms and energy barriers of the decomposition reaction of HCOOH in the gas phase [27,28]. The energy barriers are in kcal mol^{-1}.

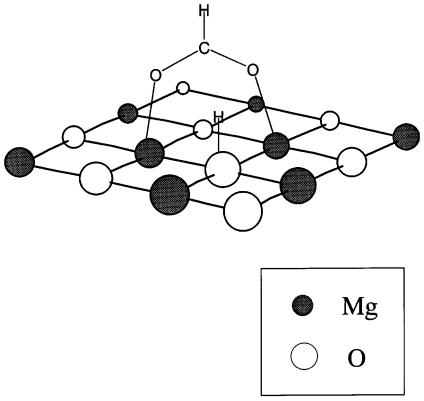

Fig. 3. The geometries of adsorbed HCOO and OH species.

conjugate base. Wu and Goodman [49] also showed that thermally generated surface defect sites with a low coordination number exhibited higher activity to surface reactions. With regard to the acquisition of adsorptive–catalytic reactivity of the surface, only high temperature dehydration has been reported [50]. This suggests that the defect site on the surface plays an important role in the decomposition reaction. In this study we examine the decomposition rections on a perfect MgO(100) surface and on surfaces having O and O^{2-} vacancies.

2. Model and calculational method

We used Mg_8O_8 clusters (Fig. 4) embedded in an electrostatic field to simulate the Madelung potential. The entire MgO model used in this study has three layers, and each layer can be expressed by $Mg_{50}O_{50}$. The Mg_8O_8 cluster is located at the center of the surface, and we put point charges at the 284 lattice sites around the Mg_8O_8 cluster. Model a is used to simulate a perfect flat surface. We previously reported the adsorption of HCOOH and the surface reaction on an MgO(100) surface using this model, and our results were consistent with experimental data [42]. Therefore, we think that this model is appropriate. Model b is used to simulate a defective surface, and the Mg_8O_8 cluster consists of two layers. We think that the defect site plays an important role as a reaction site, and

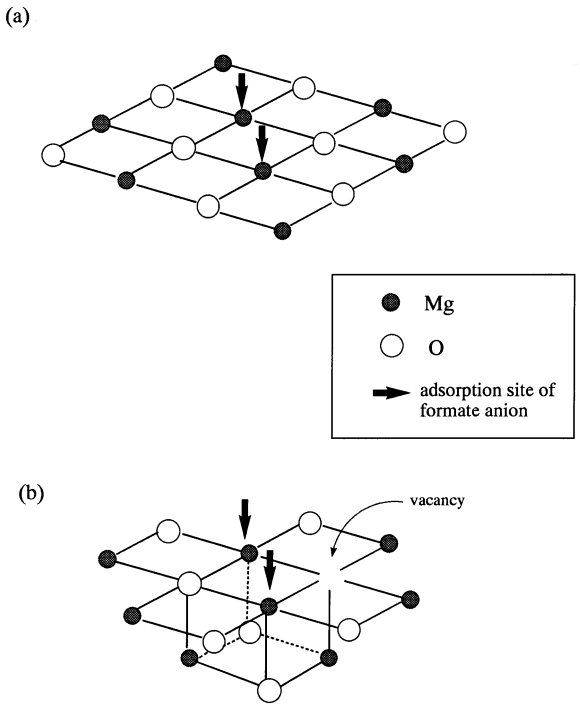

Fig. 4. Mg_8O_8 clusters as a model of the MgO(100) surface. Model a represents a part of the first layer of a MgO crystal lattice and is placed into an electrostatic field represented by 284 point charges located on the MgO crystal lattice. Model b is a part of the first and second layers of a MgO crystal lattice and is placed into an electrostatic field represented by 284 point charges located on the MgO crystal lattice. The first layer of each cluster is used for the adsorption and dissociation of HCOOH. The arrows indicate the sites for the bridging structure in formate adsorption.

an Mg atom behind the defect site would directly affect the reaction site. Therefore, we put one more layer behind the defect site. Although these clusters are small, they include all of the nearest neighbors of the reaction sites. Considering the region of the interaction between the ad-molecule and the surface, this cluster can represent the surface on which the decomposition reaction of formic acid takes place. The Madelung potential is proportional to the ionic charge, q, in $Mg_8^{q+}O_8^{q-}$ The Mulliken atomic charge of the Mg_8O_8 cluster calculated at the Hartree–Fock level is about ± 1.3–1.5, which overestimates q because of the spatial distribution of the electron cloud. We used point charges, $+1.0$ on Mg and -1.0 on O, located at the 284 lattice

sites around the Mg_8O_8 cluster. The cluster geometries are fixed at the crystal lattice positions with a MgO distance of 2.105 Å during the surface reaction processes. We expect that relaxation of the MgO surface should play an important role in adsorption and surface reactions, but the large number of degrees of freedom presents a formidable optimization problem when it comes to reaction path calculations. To simplify this task, we did not include relaxation of the MgO surface in our calculations. Only the geometries of the adsorbates were optimized using the energy gradient method.

We used the first layer of the Mg_8O_8 cluster for reaction sites. For example, bridging formic acids are assumed to be adsorbed on the Mg atoms shown by the arrows in Fig. 4. The molecular plane of the adsorbed formate species on metal and metal oxide surfaces has been reported to be perpendicular to the surface [11,24,51]. Therefore, the molecular plane of the adsorbed formic anion is fixed to be perpendicular to the surface, except when noted otherwise.

The basis set used for the Mg atom is the (3s3p)/[2s2p] set of Hay and Wadt and the Ar core is replaced by the effective core potential [52]. For C and O atoms, the (9s5p)/[4s2p] sets of Huzinaga and Dunning are used, and the (4s)/[2p] set is used for H atoms [53,54].

Restricted and unrestricted Hartree–Fock and unrestricted MP2 calculations were carried out using the program HONDO8 [55].

3. Decomposition reaction on a perfect MgO(100) surface

We first examine the decomposition reaction on a perfect flat surface using model a in Fig. 4. We assume the mechanism shown in Fig. 5. A three-membered ring, which has the same geometry as the transition state in the dehydration reaction in the gas phase, is expected to be formed in the transition state. The energy barrier of this reaction is 93.8 kcal mol^{-1}.

We next examine the role of the dynamic bending mode in the decomposition reaction. The dynamic bending mode of an adsorbed formate anion, in which it tilts toward the surface, has been observed on a Ag surface [24]. Since the C–H bond interacts more effectively with the surface by tilting of the molecular plane, this mode is expected to be important for inducing C–H bond cleavage [41]. We examined this mode on MgO(001) [42] and ZnO($10\bar{1}0$) [43] surfaces and found that the formate anion easily tilts by secondary perturbation: perturbation of only 16 kcal mol^{-1} can tilt the formate anion by 90° on a MgO(100) surface [42]. We assume that the mechanism for the decomposition has two steps, as shown in Fig. 6a. In the first step, the molecular plane of the adsorbed formate anion tilts toward the surface by 90°. In the second step, the C–H bond is assumed to cleave on the lattice O or Mg atom or the surface OH species. The C–H bond is located above the lattice O atom when the molecular plane tilts. When the C–H bond interacts with a Mg atom or OH species, the formate anion needs to move. The transfer of the formate anion while keeping the molecular plane parallel to the surface has almost no energy barrier. After the C–H bond cleaves on the lattice O or Mg atom, an adsorbed CO_2 molecule and the surface OH and MgH species are expected to be formed, respectively. When the C–H bond interacts with the surface OH species, adsorbed CO_2 and H_2O molecules are expected to be formed. However, the energy barriers are higher than 80 kcal mol^{-1} in all cases.

We previously studied formic acid decomposition on a ZnO($10\bar{1}0$) surface [44]. The formate anion rotated around the carbonyl CO bond to form the intermediate, which had a unidentate geometry, and then the C–H bond cleaved on the Zn atom. We consider the same mechanism for the MgO surface, as shown in Fig. 6b. However the energy barrier is again higher than 80 kcal mol^{-1}.

These barriers are too high for the decomposition of surface formate species. Thus, we could not find a favorable mechanism for the decomposition reaction on a perfect MgO(100) surface.

4. Decomposition reaction on surfaces with O and O^{2-} vacancies

Tsukada et al. [56] investigated the electronic structure of the defect state associated with an

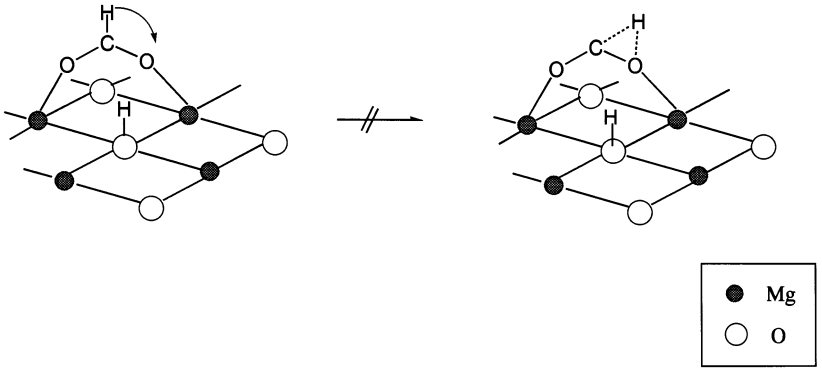

Fig. 5. Assumed decomposition path for bridging type $HCOO^-$ on a perfect MgO surface (model a).

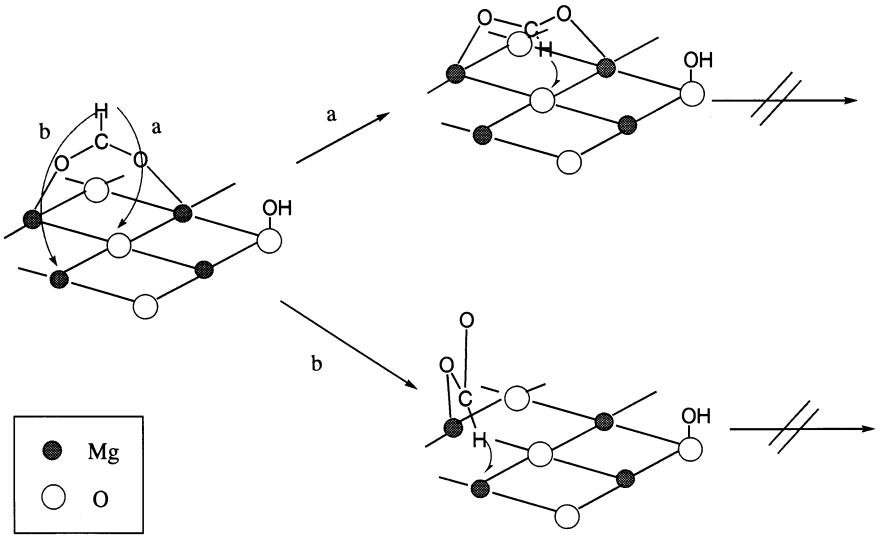

Fig. 6. Assumed decomposition path way for the bridging type $HCOO^-$ on a perfect MgO surface (model a). The C–H bond cleaves on a lattice O atom in path a, while it cleaves on a lattice Mg atom in path b.

oxygen vacancy of an MgO surface by the DV-Xα cluster method. They concluded that two charge states of the vacancy (O and O^-) are present on the MgO(100) surface. We therefore assumed the three charge states of an oxygen vacancy surface: O, O^- and O^{2-} vacancies. An O vacancy on the surface means that a lattice O atom is missing from the surface and the O^- and O^{2-} vacancies mean that lattice O atoms with one and two electrons are missing, respectively. However the O^- vacancy state had the convergence problem in our calculation of the electronic structure. We first compare the electronic structures of MgO surfaces with O and O^{2-} vacancies. The difference in electron density between the O^{2-} and O vacancies is defined by

$$\Delta\rho = \rho(O^{2-}\text{ vacancy surface}) - \rho(\text{O vacancy surface}) \quad (1)$$

and is shown in Fig. 7.

The Mg atoms located next to the vacancy, which are Mg3 and Mg4 shown in Fig. 7, are polarized towards the vacancy site. And the all O atoms, especially O1 and O2 atoms located next to the vacancy, are polarized towards the vacancy site.

We examine here all the same mechanisms as

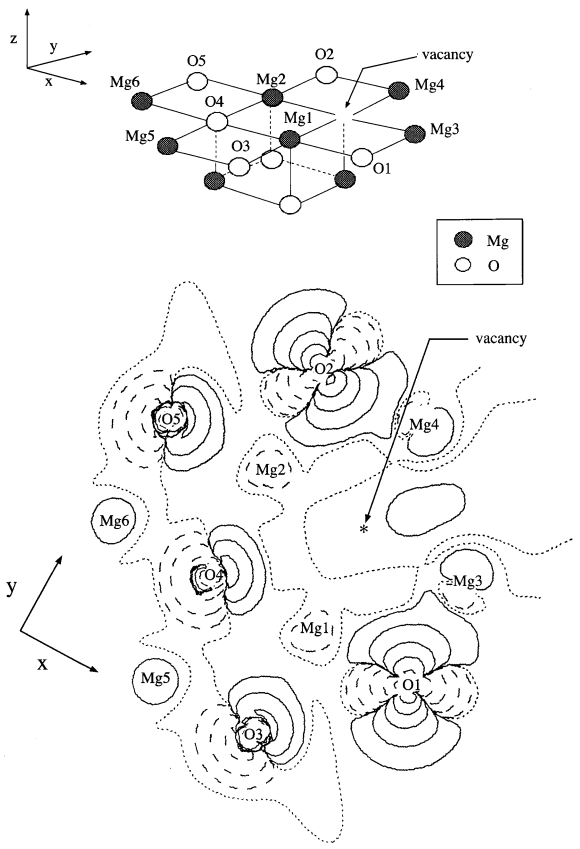

Fig. 7. The density difference between the O and O^{2-} vacancy surfaces as defined by Eq. (1) in the x–y plane. Solid, dotted and broken lines denote positive, zero and negative values of the electronic density shifts, $\Delta\rho$, respectively.

those examined in the previous section on those surfaces. The first mechanism includes the three-membered ring structure in the transition state as shown in Fig. 5. The energy barriers of this mechanism were as large as than 80 kcal mol^{-1} on both O and O^{2-} vacancy surfaces. We next examine the role of the dynamic bending mode in decomposition reaction on the vacancy surfaces. The mechanism has two steps as shown in Fig. 6a. The energy barriers on the O and O^{2-} vacancy surfaces are higher than 80 kcal mol^{-1} in all the cases where the C–H bond interacts with the Mg and O lattice atoms and the OH adsorbed species. The energy barriers for the mechanisms shown in Fig. 6b are also higher than 80 kcal mol^{-1} on the vacancy surfaces.

We next assume the mechanism shown in Fig. 8. This mechanism consists of the following two steps. In the first step, the carbonyl oxygen atom moves into the vacancy to form the intermediate shown in Fig. 8. Yamamoto et al. [57] suggested the presence of formate unidentate configuration, which has the same configuration as the intermediate in the first step of our mechanism, from the sum-frequency generation (SFG) experiment. There are then two possible paths for the second step. In path a, the C–H bond interacts with the lattice O atom. In path b, the C–H bond interacts with the lattice Mg atom. However, the interaction between the C–H bond and the lattice Mg atoms is repulsive on both surfaces, i.e. on both O and O^{2-} vacancies. Therefore, path b will not be discussed further.

We first optimize all the structures of path a in Fig. 8 by the RHF method; however the energy of the initial structure does not converge. Therefore, we discuss the energies and properties calculated by the UHF method. The energy profiles of path a on the O and O^{2-} vacancy surfaces calculated by the UHF method are shown in Fig. 9. The energy is calculated as

$$\Delta E = E - E(\text{initial structure}). \quad (2)$$

The intermediate on the O^{2-} vacancy surface is 38.9 kcal mol^{-1} more stable than that on the O vacancy surface. The energy barrier on the O^{2-} vacancy surface is 26.0 kcal mol^{-1}, while that on the O vacancy surface is 106.7 kcal mol^{-1}. The reaction on the O^{2-} vacancy surface is exothermic by 35.6 kcal mol^{-1}, while that on the O vacancy surface is endothermic by 17.2 kcal mol^{-1}.

The optimized geometries and the net charge on each atom in the intermediate and the transition state in path a are shown in Fig. 10. We first discuss the intermediate. The carbonyl C–O2 bond lengths on both O^{2-} and O vacancy surfaces are longer than that in the bridging structure (1.27 Å) [42] (initial structure shown in Fig. 8). The C–O bond becomes weaker because the carbonyl O atom forms four new bonds with the lattice Mg atoms. The carboxyl C–O1 and C–O2 bond lengths on the O vacancy surface are longer than those in the O^{2-} vacancy surface. The molecular orbital diagram of the intermediate on the O^{2-}

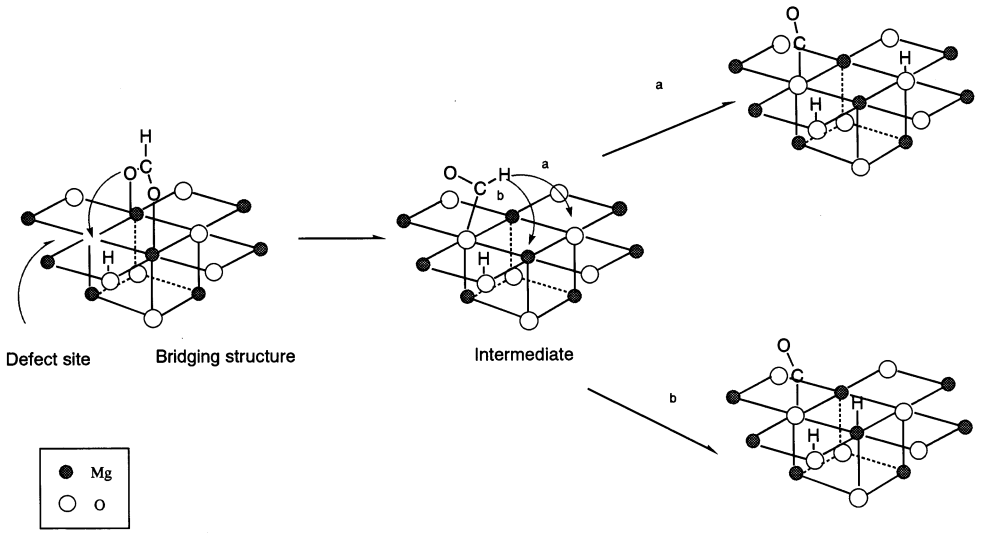

Fig. 8. Assumed decomposition path ways for bridging type $HCOO^-$ on defective MgO surfaces. The intermediate, which has a unidentate structure, is formed in the first step of both paths a and b. The C–H bond cleaves into the surface OH species and the CO molecule in path a, while it cleaves into the surface MgH species and the CO molecule in path b.

vacancy surface is shown in Fig. 11. The O–C–O π^* orbital is occupied by the one electron on the O^{2-} vacancy surface, while the O–C–O π^* orbital is filled with the two electrons on the O vacancy surface. Therefore, the C–O bond lengths on the O vacancy surface become longer. The net charge (−1.51) on the lattice oxygen atom (O3 atom in Fig. 10) on the O^{2-} vacancy surface is larger than that (−1.25) on the O vacancy surface. Therefore, we think that the lattice oxygen atom of the O^{2-} vacancy surface is more favorable as a proton acceptor than that on the O vacancy surface.

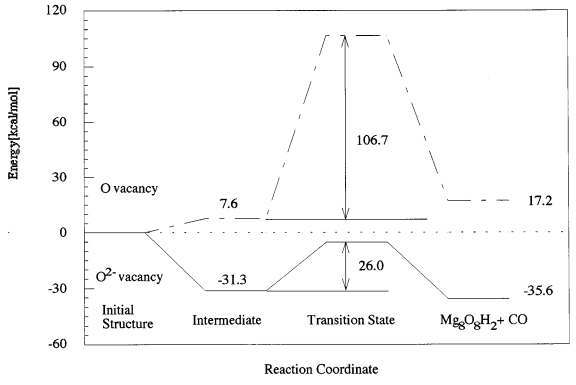

Fig. 9. Energy profiles for the formation of CO and surface OH species on the O and O^{2-} vacancy surfaces.

We next discuss the geometries of the transition state. The carbonyl C–O1 bond distance on the O^{2-} vacancy surface is close to that in the CO molecule (1.12 Å), while the C–O1 distance on the O vacancy surface is longer than that in the CO molecule. The net charge on the CO1 part of the transition state on the O^{2-} vacancy surface is slightly positive, while that on the O vacancy surface is negative. The carbonyl C–O2 bond distance on the O^{2-} vacancy surface becomes longer than that of the intermediate on the O^{2-} vacancy surface and that of the transition state on the O vacancy surface. The distance between the H and lattice O3 atoms on the O^{2-} vacancy surface is shorter than that on the O vacancy surface.

Thus, the decomposition reaction on the O^{2-} vacancy surface is favored. We found that the C–H and C–O bond cleavages occur at the same time in the transition state. The C–H bond cleaves on the lattice O atom and the H atom is pulled out as a proton to form the surface OH species. One carbonyl O atom is left on the surface to fill the vacancy site.

Yamamoto et al. [57] have reported that the

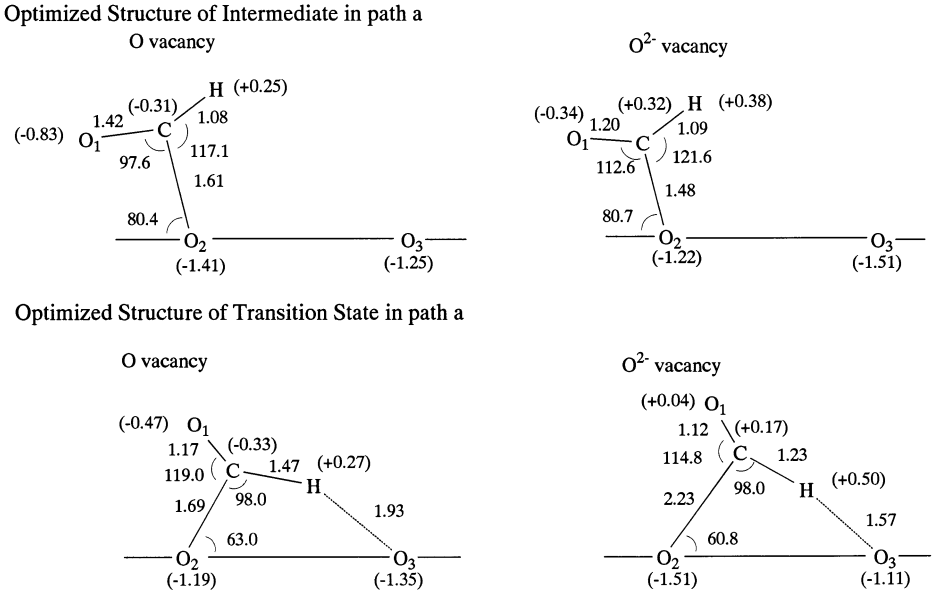

Fig. 10. Fully optimized geometrical parameters of the intermediate and the transition state on the O and O^{2-} vacancy surfaces in path a (Fig. 8). Bond distances and angles are in Å and degrees, respectively. Values in parentheses show the net atomic charge.

MgO(001) surface was roughened by the desorption of water molecules at low temperature. Xu and Koel [58] proposed that a latice oxygen was ripped off on low temperature desorption of H_2O, leaving behind an oxygen deficit site, from an acetate-covered MgO(001) surface. We therefore suggest that the surface hydrogen atom, which was produced on the dissociation of formic acid on the surface, and the lattice oxygen atom react to produce the H_2O molecule and the oxygen deficit site. The deficit oxygen site is consumed for the CO production and is reformed by the H_2O desorption.

5. Effect of electron correlation

We examined the effect of electron correlations for the decomposition path a on an O^{2-} vacancy surface (Fig. 8), which is most favorable using the UMP2 method. The geometries optimized at the HF level are used and the results are shown in Table 1. The geometries optimized at the HF level are used. The energy barrier calculated by the UMP2 method is almost the same as that at the HF level. The inclusion of electron correlations by the UMP2 method does not affect the conclusion for the decomposition reaction on the MgO surface.

6. Summary

We have studied theoretically the mechanism of the decomposition reaction of HCOOH on a Mg surface. We first found that the decomposition reaction does not occur on a perfect surface. We did not find any evidence that the dynamic bending mode of surface formate anion has an important role in the decomposition reaction on perfect and defective MgO surfaces, just as we could not find any role for this mode on a ZnO($10\bar{1}0$) surface [44].

The decomposition reaction on an O^{2-} vacancy surface is more favorable than that on an O vacancy surface. The mechanism is different from that in the gas phase. However, C–H and C–O bond cleavages occur at the same time in the transition state, as in the gas phase.

The carbonyl O atom moves into the vacancy

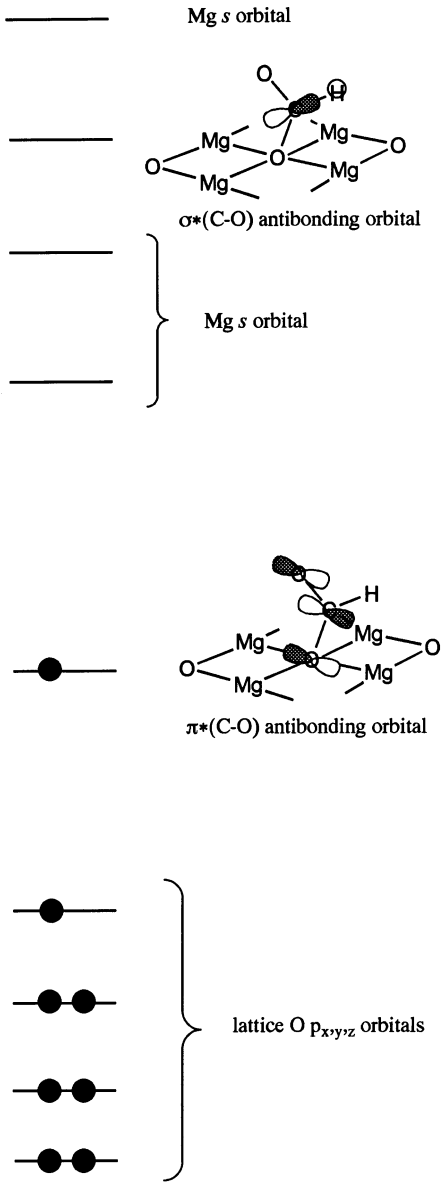

Fig. 11. Molecular orbital diagram of the intermediate on the O^{2-} vacancy surface.

to form the intermediate structure, which is 41.7 kcal mol^{-1} more stable (at the UMP2 level) than the bridging structure. The C–O bond becomes weaker because the carbonyl O atom forms four new bonds with the lattice Mg atoms.

The C–H cleaves on the lattice O atoms to form surface OH species. The interaction between the C–H and lattice Mg atoms is repulsive. One carbonyl O atom is left on the surface to fill the vacancy site. The energy barrier is 28.3 kcal mol^{-1} at the UMP2 level. The overall reaction is endothermic by 48.9 kcal mol^{-1} at the UMP2 level.

Table 1
The energy barriers ($\Delta E^{\ddagger}$) and the formation energies (ΔE) calculated at the UHF and UMP2 levels for the decomposition reaction on the O^{2-} vacancy surface

	UHF	UMP2
ΔE (intermediate structure)[a]	−31.3	−41.7
$\Delta E^{\ddagger}$ (transition state)[b]	26.0	28.3
ΔE (products)[c]	−35.6	−48.9

[a] The energy difference between the initial and intermediate structures shown in Fig. 8. The energy difference is calculated using Eq. (2).

[b] The energy barrier of path a in Fig. 8 on an O^{2-} vacancy surface. The energy difference is calculated using Eq. (2).

[c] The energy difference between the initial structure and the products shown in Fig. 8. The energy difference is calculated using Eq. (2).

Acknowledgements

We thank Professors K. Domen and C. Hirose for valuable discussions in the course of this study. We would like to thank the IMS Computer Center for allowing us to use their computer facilities to perform our calculations. This study was supported in part by the New Energy and Industrial Technology Department Organization (NEDO) and by a Grant-in-Aid for Scientific Research from the Ministry of Education, Science and Culture.

References

[1] J.M. Vohs, M.A. Barteau, Surf. Sci. 176 (1986) 91.
[2] H. Lüth, G.W. Rubloff, W.D. Grobman, Solid State Commun. 18 (1976) 1427.
[3] Y. Noto, K. Fukuda, T. Onish, K. Tamaru, Trans. Faraday Soc. 63 (1967) 3081.
[4] C.T. Au, W. Hirsch, W. Hirschwald, Surf. Sci. 199 (1988) 507.
[5] W.T. Petrie, J.M. Vohs, Surf. Sci. 245 (1991) 315.

[6] S. Akhter, W.H. Cheng, K. Lui, H.H. Kung, J. Catal. 85 (1984) 437.
[7] D.C. Foyt, J.M. White, J. Catal. 47 (1977) 260.
[8] S.H.C. Liang, I.D. Gay, J. Catal. 101 (1986) 193.
[9] N. Takezawa, C. Hanamaki, H. Kobayashi, J. Catal. 38 (1975) 101.
[10] R.O. Kagel, R.G. Greenler, J. Chem. Phys. 49 (1968) 1638.
[11] H. Yamamoto, N. Akamatsu, A. Wada, K. Domen, C. Hirose, J. Electron Spectrosc. Relat. Phenom. 64/65 (1993) 507.
[12] K. Domen, N. Akamatsu, H. Yamamoto, A. Wada, C. Hirose, Surf. Sci. 283 (1993) 468.
[13] T. Shido, K. Asakura, Y. Iwasawa, J. Catal. 122 (1990) 55.
[14] P.J. Meschter, H. Grabke, J. Metall. Trans. 10B (1979) 323.
[15] S. Sato, J.M. White, J. Am. Chem. Soc. 102 (1980) 7209.
[16] A. Ueno, T. Onishi, K. Tamaru, Trans. Faraday Soc. 67 (1971) 3585.
[17] S. Tanaka, M. Onchi, M. Nishijima, J. Chem. Phys. 92 (1989) 2712.
[18] H. Ohnish, C. Egawa, T. Aruga, Y. Iwasawa, Surf. Sci. 191 (1987) 479.
[19] S.L. Parrott, J.W. Rogers, J.M. White, Appl. Surf. Sci. 1 (1978) 443.
[20] M. Bowker, H. Houghton, K.C. Waugh, J. Chem. Soc., Faraday Trans. 77 (1981) 3023.
[21] Y.K. Sun, W.H. Weiberg, J. Chem. Phys. 94 (1991) 4587.
[22] F. Solymosi, J. Kiss, I. Kovacs, Surf. Sci. 192 (1987) 47.
[23] J.L. Falconer, R.J. Madix, Surf. Sci. 46 (1974) 473.
[24] P.A. Stevens, R.J. Madix, J. Stohr, Surf. Sci. 230 (1990) 1.
[25] K. Tanabe, M. Misono, Y. Ono, H. Hattori, New Solid Acids and Bases: Their Catalytic Properties, Elsevier, Amsterdam, 1989.
[26] X.D. Peng, M.A. Barteau, Catal. Lett. 7 (1990) 395.
[27] K. Yamashita, T. Yamabe, Int. Quantum Chem. Symp. 17 (1983) 117.
[28] K. Saito, T. Kakumoto, H. Kuroda, S. Torii, A. Imamura, J. Chem. Phys. 80 (1984) 4989.
[29] K. Sawabe, N. Koga, K. Morokuma, J. Chem. Phys. 97 (1992) 6871.
[30] J.L. Anchell, K. Morokuma, A.C. Hess, J. Chem. Phys. 99 (1993) 6004.
[31] H. Kobayashi, M. Yamaguchi, T. Ito, J. Phys. Chem. 94 (1990) 7206.
[32] E.A. Colbourn, W.C. Mackrodt, Surf. Sci. 117 (1992) 571.
[33] H. Nakatsuji, Y. Fukunishi, Int. J. Quantum Chem. 42 (1992) 1101.
[34] A.B. Anderson, J.M. Nichols, J. Am. Chem. Soc. 108 (1986) 4742.
[35] H. Nakatsuji, M. Hada, K. Nagata, H. Ogawa, K. Domen, J. Phys. Chem. 98 (1994) 11840.
[36] H. Nakatsuji, M. Hada, J. Am. Chem. Soc. 107 (1985) 8264.
[37] H. Nakatsuji, M. Hada, T. Yonezawa, J. Am. Chem. Soc. 109 (1987) 1902.
[38] H. Nakatsuji, Y. Matsuzaki, T. Yonezawa, J. Chem. Phys. 88 (1988) 5759.
[39] J. Sauer, C.M. Kolmel, J.R. Hiller, R. Ahlrichs, Chem. Phys. Lett. 164 (1989) 193.
[40] J. Sauer, J. Phys. Chem. 91 (1987) 2315.
[41] I. Pápai, J. Ushio, D.R. Salahub, Surf. Sci. 282 (1993) 262.
[42] H. Nakatsuji, M. Yoshimoto, M. Hada, K. Domen, C. Hirose, Surf. Sci. 336 (1995) 232.
[43] H. Nakatsuji, M. Yoshimoto, Y. Umemura, S. Takagi, M. Hada, J. Phys. Chem. 100 (1996) 694.
[44] M. Yoshimoto, S. Takagi, Y. Umemura, M. Hada, H. Nakatsuji, J. Catal. 173 (1998) 53.
[45] S. Coluccia, A. Barton, A.J. Trench, J. Chem. Soc., Faraday Trans. I 77 (1981) 2203.
[46] M.A. Karolewski, R.G. Cavell, Surf. Sci. 290 (1993) 80.
[47] W. Langel, M. Parrinello, Phys. Rev. Lett. 73 (1994) 504.
[48] D. Peng, M.A. Barteau, Langmuir 7 (1991) 1426.
[49] M.-C. Wu, D.W. Goodman, Catal. Lett. 15 (1992) 1.
[50] H. Dunski, W.K. Józwiak, H. Sugier, J. Catal. 146 (1994) 166.
[51] M.D. Weisel, J.G. Chen, F.M. Hoffman, Y.K. Sun, W.H. Weinberg, J. Chem. Phys. 97 (1992) 9396.
[52] P.J. Hay, W.R. Wadt, J. Chem. Phys. 82 (1985) 270.
[53] S. Huzinaga, J. Chem. Phys. 42 (1965) 1293.
[54] T.H. Dunning Jr., J. Chem. Phys. 53 (1970) 2823.
[55] M. Dupuis, A. Farazdel, MOTEC-91, Center for Scientific and Engineering Computations, IBM Corporation, 1991.
[56] M. Tsukada, H. Adachi, C. Satoko, Prog. Surf. Sci. 14 (1983) 113.
[57] H. Yamamoto, N. Watanabe, A. Wada, K. Domen, C. Hirose, J. Chem. Phys. 106 (1997) 4734.
[58] C. Xu, B.E. Koel, J. Chem. Phys. 102 (1995) 8158.